



# A highly active nanocomposite silica-carbon supported palladium catalyst for decarboxylation of free fatty acids for green diesel production: Correlation of activity and catalyst properties

Elvan Sari<sup>a</sup>, Manhoe Kim<sup>b,c</sup>, Steven O. Salley<sup>a,b</sup>, K.Y. Simon Ng<sup>a,b,c,\*</sup>

<sup>a</sup> Department of Chemical Engineering and Material Science, Wayne State University, Detroit, MI 48202, USA

<sup>b</sup> National Biofuels Energy Laboratory, NextEnergy, Detroit, MI 48202, USA

<sup>c</sup> Alternative Energy Technology, Wayne State University, Detroit, MI 48202, USA

## ARTICLE INFO

### Article history:

Received 8 May 2013

Received in revised form 17 July 2013

Accepted 23 July 2013

Available online 1 August 2013

### Keywords:

Decarboxylation

Green diesel

Fatty acid

Deoxygenation

## ABSTRACT

A class of Pd catalyst supported on a silica-activated carbon nanocomposite for free fatty acid (FFA) decarboxylation was developed, and displayed excellent activity and operation stability selectively for the green diesel hydrocarbons formation in the absence of H<sub>2</sub> under mild reaction conditions. Six catalysts containing 5 wt% Pd were prepared by systematically varying the silica content in the support. In addition to the effect of particle size, the impact of catalyst preparation method on the activity and selectivity was elucidated. A 5 wt% Pd/Si-C-4 catalyst maintained stable activity for 16 days under reaction conditions of 1.5 MPa and 300 °C. Although a continuous supply of H<sub>2</sub> was not necessary, H<sub>2</sub> treatment was essential to restore the catalytic activity and the desired product selectivity. Characterization of the catalyst revealed that the highly active Pd/Si-C-4 catalyst has easily accessible and well-distributed metallic Pd nanoparticles inside the hybrid mesopores.

© 2013 Elsevier B.V. All rights reserved.

## 1. Introduction

Environmental awareness and projected increases in the world's energy demand have been the motivation for seeking environmentally friendly, renewable alternative fuels. A large amount of waste cooking oil and grease is produced in the U.S. that can be exploited for liquid biofuel generation. In particular, brown grease, which contains mainly free fatty acids (FFAs), can be a potential inexpensive source for a process to obtain straight chain hydrocarbons in the diesel fuel boiling range (green diesel) via catalytic decarboxylation.

Recently, there has been considerable attention on the development of suitable catalysts for decarboxylation of free fatty acids (FFA) [1–6]. Most early studies focused on Pd-based catalysts, which exhibit high activity and selectivity for the formation of straight chain hydrocarbons with one carbon number less than the source FFA [7]. However, these supported palladium catalysts readily deactivate even in the presence of H<sub>2</sub>. Although a 3 wt% Pd-SBA-15 catalyst was active at 300 °C under 17 bar of 5 vol% H<sub>2</sub> in argon for stearic acid decarboxylation for 5 h, deactivation was

reported due to the formation of unsaturated heptadecene product [3]. A 1 wt% Pd supported on a synthetic mesoporous carbon catalyst showed 23% decrease in the BET specific surface area after decarboxylation of palmitic and stearic acids mixture at 300 °C and 17.5 bar H<sub>2</sub>/Ar [1]. In all cases, the extensive catalyst deactivation was attributed to catalyst coking. Snare et al. related the catalyst deactivation to the amount of unsaturated products which further led to catalyst coking specifically for Ru/C and Rh/C catalysts after 6 h of stearic acid decarboxylation [7]. On the other hand, the Pd/C catalyst deactivation was attributed to the reaction atmosphere and degree of unsaturation of the FFA by some researchers [8–10] and to catalyst supports by others [4]. Recently, the Jones group showed that the deactivation of a mesoporous silica supported palladium catalyst occurred during FFA decarboxylation due to the loss in total surface area, porosity and accessible palladium surface area [5]. Unlike the previously reported literature claim of coke formation, it was claimed that strongly adsorbed reactants and products cause the deactivation. The Savage group [11] also investigated the stability of 5% Pd/C in fatty acid hydrothermal decarboxylation, and it was reported that the decarboxylation activity of the catalysts was maintained although metal dispersion was significantly reduced after catalyst reuse. The difference in catalytic behavior of the supported metal particles was attributed to the hydrothermal reaction where the catalyst was exposed to sub-critical water.

An ordered mesoporous silica-carbon catalyst support was synthesized as a novel hybrid material [12]. This nanocomposite

\* Corresponding author at: Department of Chemical Engineering and Material Science, Wayne State University, Detroit, MI 48202, USA. Tel.: +1 313 577 3805; fax: +1 313 577 3810.

E-mail address: [sng@wayne.edu](mailto:sng@wayne.edu) (K.Y.S. Ng).

support has gained increasing attention for catalysis applications in recent years due to several unique features such as high dispersion of palladium nanoparticles (about 3 nm), high surface area, large and tunable pore structure and excellent stability [13,14]. These silica-carbon nanocomposites were produced on the basis of a triblock copolymer templating approach which is a time consuming catalyst preparation technique.

The nature of the surface functional groups on the activated carbon support when modified by oxidative treatments was found to be very important for the catalytic activity of precious metals such as palladium [15,16]. After introducing such oxygen groups, the surface behavior of carbon changes; therefore their catalytic properties differ [17]. The components of activated carbon are disorganized polyaromatic sheets with reactive corner atoms and adsorbent surface atoms. The precursor that is selected for this study, TEOS, is expected to form the templates that contain –OH groups and bridged O atoms in a Si–O–Si structure on the amorphous silica walls, and these groups play a very important role for the incorporation of silica into activated carbon.

In the present work, a new, well-defined and highly efficient Pd/Si-C catalyst was developed for the decarboxylation of FFA. This new nanostructured hybrid catalyst has a well-defined mesoporous structure which allows a better understanding of structure–activity characteristics that are crucial in elucidating the FFA decarboxylation mechanism, unlike an activated carbon supported palladium catalyst. The decarboxylation reaction of oleic acid was investigated over these catalysts with the aim of producing green diesel in the absence of additional H<sub>2</sub> under mild reaction conditions, elucidating the effects of the nature of the functional groups on the activity and developing a procedure to maintain high catalytic activity.

## 2. Experimental

### 2.1. Materials

The following chemicals were used in this investigation: a commercial activated carbon (Charcoal Norit, Sigma–Aldrich), tetraethyl orthosilicate (TEOS, 99.999%, Sigma–Aldrich), palladium(II) chloride (PdCl<sub>2</sub>, ≥99.9%, Sigma–Aldrich), oleic acid (technical grade 90%, Sigma–Aldrich, St. Louis, MO), dodecane (anhydrous, ≥99%, Sigma–Aldrich), carbon disulfide (HPLC grade ≥99.9%, Sigma–Aldrich), methyl arachidate (>99%, Nu-Chek Prep Inc., Elysian, MN), Ultra high purity grade argon (Ar), hydrogen (H<sub>2</sub>) and nitrogen (N<sub>2</sub>) were purchased from Cryogenic Gases (Detroit, MI).

### 2.2. Catalyst preparation

Activated carbon (AC) was immersed in liquid TEOS with varying mass ratios of TEOS to AC. The mixture was stirred vigorously for 2 h at 120 °C. Then, it was dried at 105 °C for 18 h. Prepared supports were designated as Si-AC-*x* where *x* represents the mass ratio of TEOS to AC. During the preparation of Si-AC-0.5 and Si-AC-1, ethanol was added to provide necessary wetness of AC. For comparison, only activated carbon and only silica supported catalysts were also prepared. A support containing only silica was prepared by calcination of the Si-AC-3 support at 550 °C for 5 h in air to remove activated carbon. In order to obtain 5 wt% Pd on the support, 1.1 wt% PdCl<sub>2</sub> solution was mixed with the support (PdCl<sub>2</sub>/support = 0.088 wt/wt) at room temperature for 24 h. After each catalyst was dried at 100 °C for 5 h, the reduction was carried out under a flow of 10 vol% H<sub>2</sub>–90 vol% N<sub>2</sub> at 200 °C for 3 h.

### 2.3. Material characterization

Powder X-ray diffraction (XRD) patterns were obtained on a Rigaku MiniFlex 600 at a scan rate of 3°/min (40 kV, 15 mA). The Scherrer equation and Bragg's law were used to calculate the mean metal particle size and the lattice parameter, respectively.

A Brunauer–Emmett–Teller (BET) analysis was carried out using a Micromeritics TriStar II 3020 (V1.03) surface area analyzer. The samples were degassed in vacuum (P) at 200 °C for 6 h prior to analysis. The adsorption/desorption isotherms were acquired at 87.30 K in the relative pressure range of 0.01–0.99. The Barrett–Joyner–Halenda (BJH) model was used to derive the pore volumes, average pore diameters and pore size distributions from the desorption branches of the isotherms. A *t*-Plot was used to calculate the micropore surface areas and micropore volumes.

Catalyst acidity was determined with a Brinkmann/Metrohm 809 Titrand (Westbury, NY) potentiometric titrator. An acid–base technique [18] was performed to determine the total acid number of surface groups reacted in the catalyst slurry of 0.1 g catalyst and 75 mL titration solvent including a mixture of water, propan-2-ol and toluene. A solution containing 0.1 N KOH was used as titrant. The amount of titrant consumed to reach a potentiometric end point (EP) was used to calculate the amount of acidic groups.

Transmission electron microscopy (TEM) was conducted using a JEM-2010 microscope operating at 200 kV. The catalysts that were suspended in ethanol were placed on a carbon coated copper grid.

Fourier transform infrared (FTIR) spectra of powder catalysts were collected on a Spectra 400 spectrometer (Perkin-Elmer, Shelton, CT). Four scans were used to establish an acceptable signal to noise level for each spectrum.

### 2.4. Decarboxylation procedure

#### 2.4.1. Batch reactions

The liquid-phase decarboxylation of oleic acid was investigated in a 100 mL Hanwoul (Geumjeong-dong, South Korea) stirred batch reactor. Gas flow rates were controlled by Brooks (Warren, MI) metal sealed mass flow controllers. In all experiments, the catalyst was soaked in dodecane (solvent) prior to the reduction of the catalyst under H<sub>2</sub> flow of 60 mL/min [10]. During the reduction step the agitation speed was kept at 250 ± 2 rpm, and the pressure was 0.5 MPa. As soon as the desired pressure was reached, the temperature was increased to 200 °C with a temperature ramp of 10 °C/min and kept under flowing H<sub>2</sub> for 1 h at 200 °C. After cooling the reactor under H<sub>2</sub> flow, excess H<sub>2</sub> was purged with inert gas and oleic acid was fed into the vessel through a one way valve.

For the activity test of each catalyst, 0.45 g catalyst, 2.0 g oleic acid and 30.0 g solvent were used. Throughout the reaction, the agitation speed was kept at 1000 ± 4 rpm. Ar gas was added into the vessel in order to obtain 1.5 MPa total pressure at 300 °C. After the reaction, the reactor was quenched in an ice bath and the final liquid product was analyzed. The standard deviation for conversion and product selectivities from a multiple run control experiment was ±2.4%.

#### 2.4.2. Flow reactor

The continuous decarboxylation of brown grease was carried out in a fixed bed tubular reactor (40 mL BTRS-Jr, Autoclave Engineers, PA). Two grams of catalyst was placed between glass wool layers. The catalyst was first reduced at 200 °C and 0.5 MPa under H<sub>2</sub> flow. After reduction, the reactor was pressurized to 1.5 MPa under Ar gas and heated to 300 °C. Oleic acid (0.2 M in dodecane) was continuously fed through the catalyst bed at a volumetric flow of 0.04 mL/min.

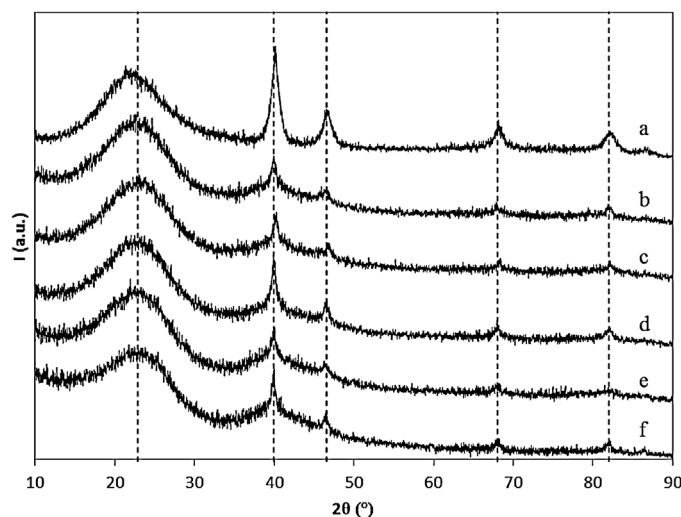


**Fig. 1.** Wide-angle XRD patterns of fresh palladium catalysts supported on: silica (a), Si-C(4:1) (b), Si-C(2:1) (c), Si-C(1:1) (d), Si-C(0.5:1) (e), activated carbon (f).

### 2.5. Analysis method

Liquid samples products were dissolved in carbon disulfide and were analyzed using a Perkin-Elmer Clarus 500 gas chromatograph (GC) equipped with flame ionization detector (FID) and an Rtx-65 TG column (length: 30 m, internal diameter: 0.25 mm, phase film thickness: 0.10  $\mu\text{m}$ ). The GC oven temperature was programmed as follows: 2 min hold at 80 °C, 10 °C/min ramp to 300 °C, 10 min hold at 300 °C. The detector temperature was maintained at 300 °C. Samples (1  $\mu\text{L}$ ) were injected into the column with a 50:1 split ratio, and concentrations were determined relative to a methyl arachidate internal standard. In order to identify some of the products, a GC-MS (Clarus 500 GC-MS, Perkin-Elmer) with a capillary wax Rtx-WAX column (length: 60 m, diameter: 0.25 mm, thickness of stationary phase 0.25  $\mu\text{m}$ ) was also used.

## 3. Results and discussion

### 3.1. Change in the catalyst structure and the nature of surface groups

The XRD patterns of the fresh palladium catalysts supported on activated carbon, silica and Si-C with four different silica to carbon ratios are shown in Fig. 1. For all catalysts except Pd/Si, a broad peak at  $2\theta$  of 23.9° and an overlapped broad peak at about 39.8° were observed, which correspond to the (002) and (100) diffractions of amorphous carbon for Pd/C, respectively [19]. The  $d$  spacing of the (002) plane is 0.37 nm for Pd/C which is greater than that of graphitic carbon (0.343 nm), indicating that this catalyst does not contain graphitic carbon [20]. For the Pd/Si catalyst, the broad peak at 22.0° corresponds to amorphous silica [21]. The (002) amorphous carbon diffraction shifted from 23.9° to 23.0° as the Si amount increased. Several well-resolved peaks at  $2\theta$  of 40°, 47°, 68° and 82° that are assigned to the (111), (200), (220), and (311) reflections of the face-centered cubic (fcc) Pd lattice are observed in the XRD pattern of samples. Only in the Pd/Si-C-0.5 catalyst, Pd(311) diffraction was not observed. The palladium particle size calculated from the Scherrer formula for each catalyst is 6.7, 5.5, 5.9, 6.3, 6.2 and 4.1 nm for Si, Si-C-4, Si-C-2, Si-C-1, Si-C-0.5 and C supported Pd catalysts, respectively. The larger metal particle sizes for the silica modified samples compared to the activated carbon supported catalyst may be attributed to the nature of the surface groups on the support. It is believed that small metal

particles agglomerate to larger particles because they become mobile on the surface when the surface groups thermally decompose during the metal reduction [22].

The TEM images of the fresh palladium catalysts supported on silica, Si-C-4, Si-C-2, Si-C-1, Si-C-0.5 and activated carbon are given in Fig. 2(a)–(f). The TEM image of the Pd/Si catalyst (Fig. 2(a)) displays a large distribution of sintered Pd particles with an average particle size of 5.3 nm. The larger particle size of Pd/Si catalyst may be due to the lower surface area of Si support and suggests that Pd particles were not stabilized by the oxide support [23]. The inset of the Fig. 2(a) shows the large silica particles with about 100 nm. Pd/Si-C-4 has fairly narrow Pd particle size distribution with average particle size of 3.0 nm (Fig. 2(b)). The Pd metal appears to be clustered together rather than being spherical in Si-C-1 and Si-C-0.5 (Fig. 2(d) and (e)). TEM image of Pd/C (Fig. 2(f)) shows very fine Pd particles. All the particle sizes observed by TEM images were slightly smaller than those are evidenced by XRD. Nevertheless, both TEM and XRD data confirmed the existence of sintered Pd particles in the Si, Si-C-1 and Si-C-0.5 supported catalysts.

Fig. 3 shows that all the catalysts display type-IV  $\text{N}_2$  isotherms which is associated with monolayer–multilayer adsorption and capillary condensation taking place in mesopores. An  $\text{H}_4$ -type hysteresis loop is also evident, which is often associated with the presence of mesopores with narrow slit-like pores [24]. With increasing carbon content of the support, more obvious hysteresis loops are observed (Fig. 3(d)–(f)). The capillary condensation step shifts to a lower relative pressure in a range of  $P/P_0 = 0.44$ –0.92 for the Pd/Si catalyst, which is related to the pore size reduction to 3.6 nm. This is likely due to shrinkage of the support's framework during the calcination at 550 °C. The silica mesostructure may possibly have been destroyed during the carbon combustion from the Si-C-3 support. Pore size distribution curves of Si-C supported catalysts with different Si content (Fig. 4) shows a narrow pore size distribution. The Pd/Si shows bimodal-pores centered at 2.6 and 3.8 nm.

The activated carbon support has a high surface area and a well-developed porosity, with most of the surface area in the micropores. In the modified material, the sol–gel preparation of Pd/Si-C-1 and Pd/Si-C-0.5 (in the presence of ethanol) led to a significant decrease in the micropore volume as well as surface area (Table 1). This can be attributed to pore blockage by the silica particles. On the other hand, the silica content did not contribute to a significant change in the micropore volume of catalysts Pd/Si-C-4 and Pd/Si-C-2. As silica content increases in the support, the BET surface areas and total pore volumes decrease gradually. Yet the average pore diameters do not follow the same trend. For Si-C-2 and Si-C-4 supported catalysts, the pore sizes remain nearly constant at about 5.3 nm, which is the same as that of Pd/C, after Si addition to C. However, pore sizes greatly decreased in Pd/Si-C-0.5 and Pd/Si-C-1, which may be due to blockage of larger pores. This pore blockage may be due to hydrolysis of TEOS in the presence of ethanol–water mixture followed by a condensation that takes place between a silanol and ethoxy group [25]. Bridging oxygen or siloxane group (Si–O–Si) forms as a result of these reactions where ethanol was used as a solvent during the catalyst preparation. Another explanation for the extensive reduction in pore volumes of Pd/Si-C-1 and Pd/Si-C-0.5 can be due to the silica products covering the micropores of activated carbon. This is possible with the addition of ethanol which causes dissolution of TEOS and subsequent absorption by the micropores of activated carbon during the preparation of Si-C-1 and Si-C-0.5. Capillary condensation may also contribute to this process, which causes the TEOS to more rapidly go deeper inside the pores. This is in contrast to catalysts Pd/Si-C-4 and Pd/Si-C-2 where ethanol was not used and the silica precursor did not fill the micropores. In the absence of ethanol, TEOS is immiscible with water, and the hydrolysis of TEOS does not occur. In this case, thermal



**Table 1**  
Physicochemical properties.

Catalyst	$S_{\text{BET}}$ ( $\text{m}^2/\text{g}$ )	$S_{\text{m}}$ ( $\text{m}^2/\text{g}$ )	$V_{\text{t}}$ ( $\text{cm}^3/\text{g}$ )	$V_{\text{m}}$ ( $\text{cm}^3/\text{g}$ )	$\Delta V$ ( $\text{cm}^3/\text{g}$ )	$D_{\text{BJH}}$ (nm)
Pd/Si	540	–	0.444	–	–	3.6
Pd/Si-C-4	603	381	0.430	0.206	0.224	5.3
Pd/Si-C-2	637	383	0.466	0.211	0.255	5.4
Pd/Si-C-1	717	308	0.544	0.175	0.369	4.5
Pd/Si-C-0.5	882	335	0.730	0.187	0.543	4.7
Pd/C	1002	363	0.941	0.206	0.735	5.3

$S_{\text{BET}}$ , BET surface area (*t*-Plot);  $S_{\text{m}}$ , micropore surface area (*t*-Plot);  $V_{\text{t}}$ , total pore volume of pores at  $P/P_0 = 0.985$ ;  $V_{\text{m}}$ , micropore volume (*t*-Plot);  $\Delta V$ , the difference between total and micro pore volumes (mesopore volume);  $D_{\text{BJH}}$ , pore diameter (BJH desorption average pore diameter (4 V/A)).

decomposition of TEOS to form amorphous  $\text{SiO}_2$  is expected with activation energy of  $-26 \text{ kJ/mol}$  while acetaldehyde, formaldehyde, carbon dioxide, water and carbon monoxide formed as decomposition products [26]. TEOS can be completely adsorbed on activated carbon, but not its decomposition products [27]. The possibility of a complete hydrolysis of  $\text{Si}(\text{OC}_2\text{H}_5)_4$  to  $\text{Si}(\text{OH})_4$  to give silicic acid was also considered for Pd/Si-C-0.5 and Pd/Si-C-1. However, such OH groups were not detected in FTIR analysis.

Another characteristics of an activated carbon is the surface oxygen groups which determine the hydrophilic/hydrophobic properties of carbon support and make the surface acidic, basic or neutral [28]. These surface groups play a very important role in the dispersion of the active phase, and thus in catalytic activity [29]. The nature of the surface groups was identified by FTIR (Fig. 5). None of the samples showed the  $2900\text{--}3800 \text{ cm}^{-1}$  OH absorption stretching band which is associated with hydroxyl groups. However, the development of the  $960 \text{ cm}^{-1}$  Si–OH stretching band was observed in Pd/Si-C-4 and Pd/Si-C-2. The formation of the silica-carbon nanocomposites may be followed by the appearance of asymmetric stretching vibrations of Si–O–Si bonds, while incomplete condensation may be revealed by the presence of Si–OH groups [30]. The dominant peak, located at  $1056 \text{ cm}^{-1}$  in Pd/Si, is due to the Si–O–Si stretching absorption [31]. Although the frequency of the Si–O–Si stretching band increased in Si-C supported catalysts up to  $1085 \text{ cm}^{-1}$ , it did not change with the Si content of the catalyst. However, the intensity of the peak at  $1056\text{--}1085 \text{ cm}^{-1}$

increased significantly with increased Si content [13]. A broad band between  $1300$  and  $950 \text{ cm}^{-1}$  in the Pd/C spectra has a maximum at  $1180 \text{ cm}^{-1}$  (C–O stretching in acids, alcohols, phenols, ethers and esters) [32] and a shoulder at  $991 \text{ cm}^{-1}$ . Absorption in this region is usually found in oxidized carbons [33]. Solum et al. [34] reported the appearance of a band at  $1203 \text{ cm}^{-1}$  due to the formation of phosphoric acid esters. Due to the overlap of absorption bands from Si–O in this region, an unambiguous assignment is difficult. For Pd/Si-C-0.5, C–O stretching vibration ( $1215 \text{ cm}^{-1}$ ) is higher than that for Pd/C ( $1180 \text{ cm}^{-1}$ ). Such higher absorption frequency is observed in lactones which can be seen as the condensation product of an alcohol group –OH and a carboxylic acid group –COOH [35]. This absorption is not seen for the Si, Si-C-4 and Si-C-2 supported catalysts. The spectra (except for the Pd/Si) have a band between  $1600$  and  $1580 \text{ cm}^{-1}$  due to C=C aromatic ring stretching vibrations enhanced by polar functional groups. While its intensity decreases with increasing Si amount, a small shift in Pd/Si-C-4 and Pd/Si-C-2 indicates an enlargement of the aromatic ring structure [36]. The intensity of aromatic bands is lower for Pd/Si-C-0.5 and Pd/Si-C-1 catalysts than Pd/C while these bands are not seen in Pd/Si-C-2, Pd/Si-C-4 and Pd/Si. This may suggest that substitution of C–H bonds in the aromatic structure takes place and new C–R bonds form for the latter catalysts. For Pd/C, the absorptions at  $1702 \text{ cm}^{-1}$  (C=O stretch) and  $759 \text{ cm}^{-1}$  is due to C–H out of plane bending [32]. The C=O stretch frequency is lower than that of a normal ester which is  $\sim 1740 \text{ cm}^{-1}$ . This change in the C=O stretch frequency can be due to an unsaturation adjacent to the C–O– or  $\alpha$  to the C=O [32]. It can also explain the reason why its frequency is higher ( $1729 \text{ cm}^{-1}$ ) for Pd/Si-C-0.5 that that of Pd/C. The weak intensity of the C=O stretching vibration ( $1702 \text{ cm}^{-1}$ ) of Pd/Si-C-4 and Pd/Si-C-2 suggests that these two catalysts contain a small amount of carboxyl groups compared with Pd/C, Pd/Si-C-0.5 and Pd/Si-C-1. The main observation is that both Pd/Si-C-0.5 and Pd/Si-C-1 have similar surface groups to the Pd/C. On the other hand, Si, Si-C-4 and Si-C-2 supported catalysts do not contain these interactions.

The FTIR spectra of the activated carbon, Si-C-4 and silica supports are shown in Fig. 6. The activated carbon support has a broad band between  $1000$  and  $1300 \text{ cm}^{-1}$  which is assigned to CO bonds such as those exist in ethers, phenols, acids and esters [36,37]. It has another broad band between  $1500$  and  $1750 \text{ cm}^{-1}$  that can be assigned to carboxyl groups, quinones, ketones, lactones, diketone and keto-ester, and keto-enol [36,37]. The weak absorptions between  $700$  and  $950 \text{ cm}^{-1}$ , assigned to aromatic structures substituted with out-of-plane deformation mode of C–H in variously substituted benzene rings by aliphatic groups [36], appear in the spectra of the AC, but they are absent in Si and Si-C-4 samples. The AC and Si-C-4 supports have 2 bands at  $1580$  and about  $1700 \text{ cm}^{-1}$  due to the C=C stretching vibrations in aromatic rings enhanced by polar functional groups [36,37]. However, these absorptions have lower intensity for the Si-C-4. The presence of a band at about  $1700 \text{ cm}^{-1}$  may be due to the C=O stretching in carboxylic acid groups, esters, lactones and quinones [37]. The AC support spectrum shows a wide absorption band at  $3600\text{--}3200 \text{ cm}^{-1}$  with a maximum at  $3404 \text{ cm}^{-1}$ . This band can be

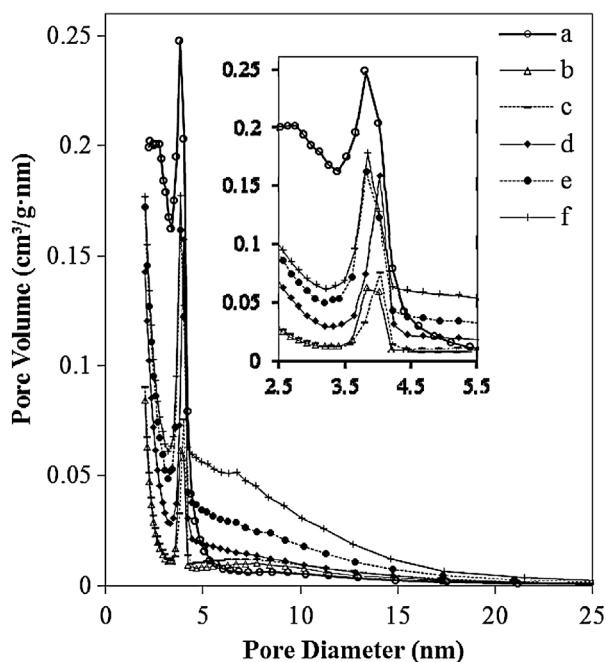


**Fig. 4.** Pore size distribution curves of palladium supported on: silica (a), Si-C(4:1) (b), Si-C(2:1) (c), Si-C(1:1) (d), Si-C(0.5:1) (e), activated carbon (f).

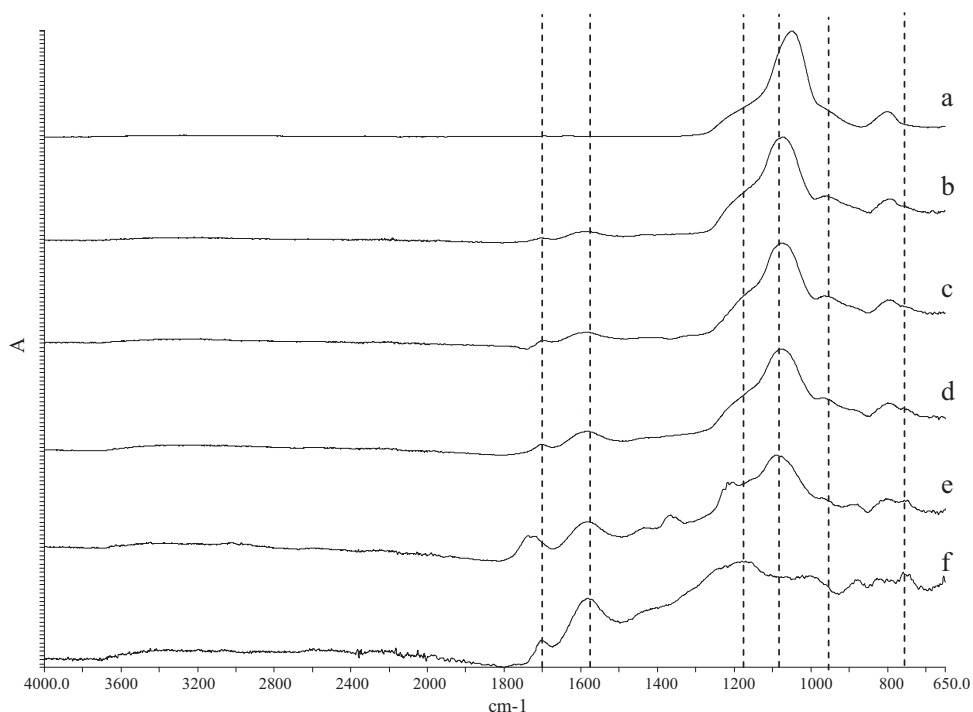


Fig. 5. FTIR of fresh palladium catalysts supported on: silica (a), SiC-4 (b), SiC-2 (c), SiC-1 (d), SiC-0.5 (e) and activated carbon (f).

assigned to the O–H stretching of hydroxyl groups such as alcohols, phenols and adsorbed water [36]. This band is more intense for AC than for Si-C-4 and Si.

The FTIR spectra for the used catalysts are shown in Fig. 7. The absorption bands are similar to the fresh catalyst (Pd/Si-C-4) after reactions but differences are in the relative intensities. The absorption bands at 2867 and 2919  $\text{cm}^{-1}$  are observed only in the used catalysts. These peaks can originate from C–H stretching in  $\text{CH}_2$  groups [36,37] likely due to the adsorbed reaction products.

The acid–base titration method gives more information on oxygen surface functionality of the catalysts. According to Boehm [38] the weakly acidic phenolic hydroxyl groups and strongly acidic carboxylic groups are neutralized by NaOH. Therefore, the total acidity is determined by neutralization. The total acid numbers of the catalysts are given in Table 2. The activated carbon supported catalyst shows some acidity which can originate from the surface oxygen groups and also from the storage conditions [17]. When the acidic groups exist on the carbon surface, it becomes more accessible for

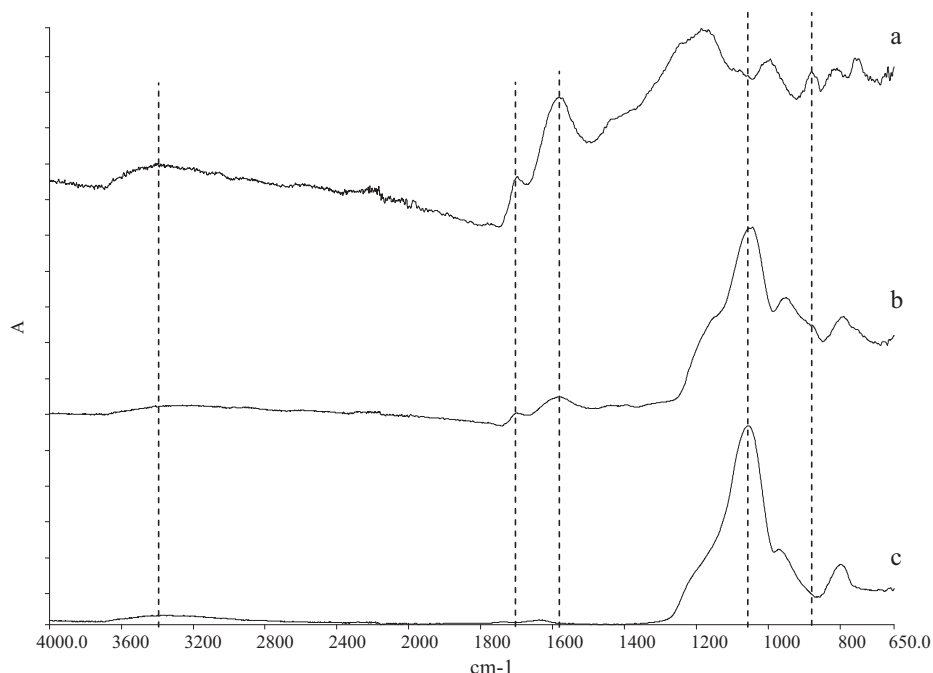


Fig. 6. FTIR of supports: activated carbon (a), Si-C-4 (b) and silica (c).

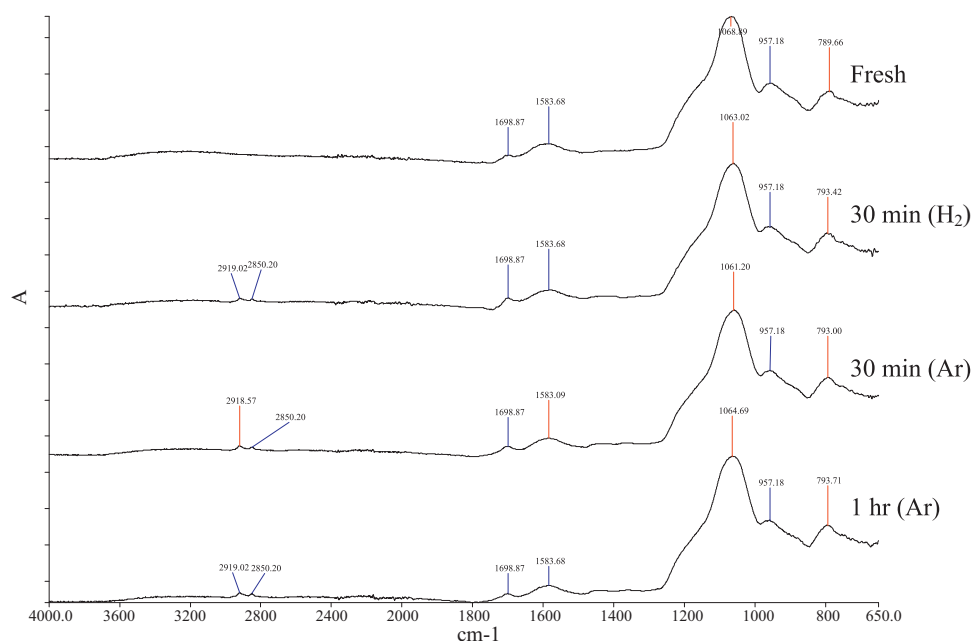


Fig. 7. FTIR of the Pd/Si-C-4 catalyst before and after oleic acid batch reaction at 300 °C and 1.5 MPa.

**Table 2**  
Acidity of supported 5% palladium catalysts.

Catalyst	Acidity (mmol/g <sub>cat</sub> )
Pd/Si	2.36
Pd/Si-C-4	0.34
Pd/Si-C-2	0.33
Pd/Si-C-1	1.53
Pd/Si-C-0.5	0.12
Pd/C	1.65

aqueous metal precursors due to the decrease in the hydrophobicity of the carbon [28]. The Pd/Si catalyst shows the greatest oxygen group content, with a predominant presence of stronger acidic groups. The Pd/Si-C-0.5 catalyst displayed the lowest total acidity.

### 3.2. Relationship between catalyst support, physicochemical properties, acidity and catalytic activity

The silica modification of the activated carbon surface produced significant changes in carbon porous texture and the surface chemistry; thus it can have dramatic effects on the catalytic activity. The analysis of the surface functionality by FTIR shows that the novel Pd/Si-C-4 catalyst has fewer surface interactions than the Pd/C catalyst, which makes it a more inert support.

Table 3 shows the correlation between Pd particle size and the catalytic properties for oleic acid decarboxylation. Both Pd/Si-C-4 and Pd/C showed high conversion of oleic acid while Pd/Si-C-4 exhibited the highest selectivity (31%) to *n*-heptadecane (*n*-C17). A high conversion of oleic acid was also observed for the Pd/Si-C-4 catalyst. However, the ability of Pd/Si in activating oleic acid to give a significant selectivity of the desired hydrocarbon products was inconsiderable (Table 3). According to the TEM, XRD and FTIR the catalysts Pd/Si-C-1 and Pd/Si-C-0.5 have similar morphology, particle size and surface groups. These catalysts exhibit similar catalytic activity for the decarboxylation of oleic acid, which indicates that the particle size of Pd can influence the catalytic activity. The high activity of Pd/Si-C-4 catalyst can be attributed to accessible, small and well-distributed metallic Pd nanoparticles inside hybrid mesopores. In addition, having low acidity and less surface

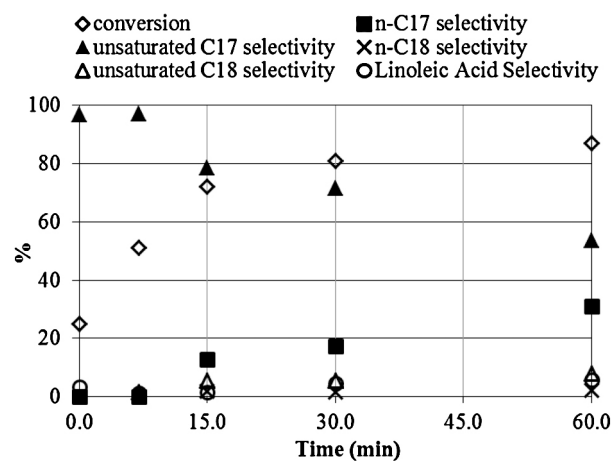


Fig. 8. Oleic acid conversion and product selectivity in batch reaction at 300 °C, 1.5 MPa on Pd/Si-C-4 catalyst.

interaction on Pd/Si-C-4 catalyst rendered it more inert and led to higher catalytic activity.

### 3.3. Decarboxylation activity of Pd/Si-C-4 in the absence of H<sub>2</sub>

The dependence of the reactant conversion and product selectivity as a function of reaction time at 15 bar and 300 °C over 5% Pd metal supported on Si-C-4 are displayed in Fig. 8. At the beginning of the reaction, unsaturated C-17 selectivity was almost 100%. When conversion reaches about 80%, unsaturated C-17 selectivity decreased and saturated *n*-C17 selectivity increased. This indicates that the C=C double bond hydrogenation is taking place after decarboxylation of oleic acid under the reaction conditions. Unlike Pd/C, which was reported to catalyze the oleic acid C=C bond via hydrogenation prior to decarboxylation of the resultant saturated FFA (stearic acid) [39], Pd/Si-C-4 catalyst follows a different reaction route. This hybrid Si-C supported Pd catalyst favors a direct decarboxylation of oleic acid instead of C=C double bond hydrogenation. By eliminating the hydrogenation of oleic acid, the reaction steps are reduced. The selectivity to stearic acid was less

**Table 3**  
Correlation between Pd particle size and catalytic properties in oleic acid decarboxylation. Batch reaction for 1 h.

5%Pd catalyst	$d_{Pd}$ (nm)	C18:1 conversion (%)	Selectivity (%)						
			C18:0	C18:2	<i>n</i> -C17	Unsaturated C17	<i>n</i> -C18	Unsaturated C18	Others*
Si	6.7	15	<0.05	<0.05	0.0	1.0	0.0	0.0	99
Si-C-4	5.5	87	<0.05	5.6	31.0	53.5	2.2	7.7	<1
Si-C-2	5.9	74	15.0	5.4	13.4	56.7	1.9	7.7	<1
Si-C-1	6.3	42	3.5	19.8	11.6	35.6	0.9	3.5	25.1
Si-C-0.5	6.2	45	2.1	22.5	12.6	32.7	1.3	3.8	25
C	4.1	94	<0.05	1.8	19.2	71.7	1.6	5.7	0

$d_{Pd}$ , Pd metal particle size (XRD).

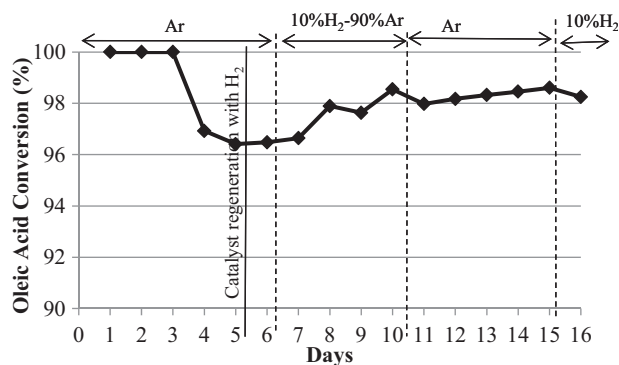


**Fig. 9.** Oleic acid conversion in flow reaction at 300 °C, 1.5 MPa on Pd/Si-C-4 catalyst with LHSV 1 h<sup>-1</sup>.

than 0.05 wt% even after 1 h reaction over Pd/Si-C-4 (Table 3) while Pd/C is reported to have 60% selectivity to stearic acid at 74% conversion of oleic acid [39]. The existence of 8 and 1-heptadecenes was also identified with GC-MS. The formation of 8-heptadecene suggests the direct decarboxylation of oleic acid while formation of 1-heptadecene indicates the dehydrogenation of *n*-heptadecane and decarbonylation of oleic acid.

### 3.4. Stability of catalyst

The stability of the Pd/Si-C-4 catalyst was investigated in a continuous flow reactor. The oleic acid conversion over 16 days of operation is shown in Fig. 9. Although there is a slight decrease in conversion after 3 days of reaction, the addition of 10% H<sub>2</sub> to the gas stream restored the conversion back to 100%. While the catalyst is stable for conversion of oleic acid for 16 days over Pd/Si-C-4 catalyst, there is a dramatic decrease in diesel hydrocarbon (HC) selectivity after 3 days of reaction (Fig. 10). After introducing 10%

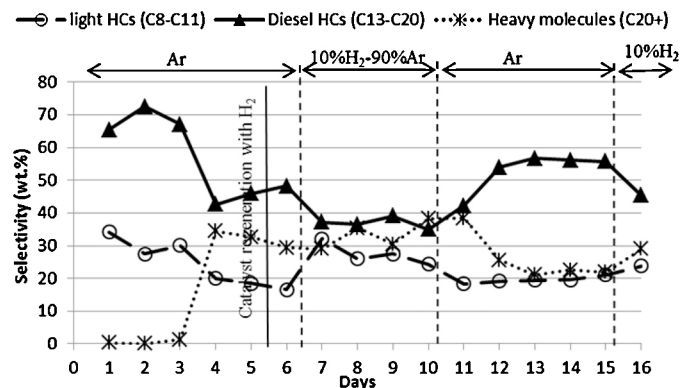


**Fig. 10.** Product selectivity in flow reaction of oleic acid at 300 °C, 1.5 MPa on Pd/Si-C-4 catalyst with LHSV 1 h<sup>-1</sup>.

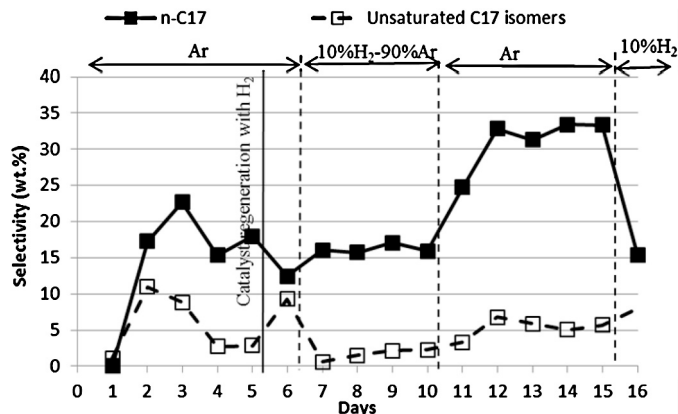


**Fig. 11.** *n*-C17 (saturated) and unsaturated C17 isomers selectivity in flow reaction of oleic acid at 300 °C, 1.5 MPa on Pd/Si-C-4 catalyst with LHSV 1 h<sup>-1</sup>.

H<sub>2</sub> in the gas stream for 4 days, diesel HC selectivity increased to 55%. This selectivity was maintained in the absence of H<sub>2</sub>. However, switching the gas flow back to 10% H<sub>2</sub>–90% Ar resulted in a decrease in diesel selectivity. Fig. 11 shows the impact of removing the H<sub>2</sub> from input on the selectivity of decarboxylation products (*n*-C17 and unsaturated C17 isomers). It is clearly seen that switching back to an Ar gas stream yields double the *n*-C17 selectivity. Murzin's group indicated that the presence of H<sub>2</sub> in small quantities in the liquid phase helps to preserve the activity of the Pd/C catalyst. However, the silica modified AC supported Pd catalyst stability study showed that the addition of 10% H<sub>2</sub> does not necessarily favor the formation of decarboxylation products, but an H<sub>2</sub> treatment helped to regenerate the decarboxylation sites of the catalyst. Recently, Lamb et al. [40] studied the effect of adsorbed hydrogen on Pd(1 1 1) surface of a palladium cluster to the gas phase decarboxylation of butanoic acid, and showed that the adsorbed surface intermediate, C<sub>2</sub>H<sub>5</sub>–CH–COO, forms propylidene in the absence of adsorbed H while –C<sub>3</sub>H<sub>7</sub> is formed in the presence of adsorbed Ziemecki observed the decomposition of the bulk PdC<sub>x</sub> phase of Pd/C at 150 °C in H<sub>2</sub> [41] and this decomposition was observed at 427 °C in an inert atmosphere by others [42]. Such regeneration can help if the interstitial C in the Pd crystallites forms during the reaction. However, the XRD study of used Pd/Si-C-4 catalyst revealed that there is no lattice expansion after reaction which would indicate the presence of a PdC<sub>x</sub> phase. In the light of the previous research and results presented in Fig. 10, a regeneration step to remove the adsorbed reactants from the active metal surface can be suggested instead of a continuous H<sub>2</sub> feed into the system. In a liquid phase fatty acid decarboxylation on a 5% Pd/C catalyst, it was similarly shown that optimum H<sub>2</sub> amount is necessary to keep the decarboxylation activity high because higher H<sub>2</sub> partial pressure causes a switch in the reaction mechanism from decarboxylation to decarbonylation [43]. The authors reported an irreversible deactivation

in the decarboxylation sites. However, Fig. 10 clearly shows that the novel Pd/Si-C catalyst's decarboxylation activity was restored after the H<sub>2</sub>-treatment (after Day-10).

The Pd/Si-C-4 catalyst maintained the highest reported conversion up to 16 days on stream toward selective decarboxylation of FFA on a supported Pd catalyst under similar reaction conditions without assistance of H<sub>2</sub> input. For example, Pd/C (Sibunit) catalyst showed stable activity only up to 45 h by maintaining 15% conversion of concentrated stearic acid at 360 °C under 1 MPa 5 vol% H<sub>2</sub> in argon while a commercial Pd/C catalyst maintained its stability up to 92 h at 40% conversion [9]. A mesoporous 1% Pd/C (egg-shell) catalyst was deactivating slowly and was rather stable at around 10% conversion up to 5 days at a 0.5 mol/L saturated FFA feed with WHSV 1.7 h<sup>-1</sup> [8].

#### 4. Conclusions

A novel process was proposed for nanocomposite silica-carbon supported catalyst synthesis in which precursors of the raw materials are mixed with activated carbon powder. The characteristic of this technique is to employ a low-temperature procedure which saves energy and time in the catalyst preparation.

The decarboxylation activities of different amount of silica containing catalysts were investigated in a batch reactor under inert gas. Among them, the formulation with the fewer oxygen surface groups (less carboxyl group, C=O) (Pd/Si-C-4) was the most active catalyst for the decarboxylation of an unsaturated FFA in the absence of H<sub>2</sub>. The high activity of the Pd/Si-C-4 catalyst is attributed to its accessible and well-distributed metallic Pd nanoparticles inside hybrid mesopores as well as to its low acidity, weak surface interactions and inertness. The novel catalyst was capable of catalyzing a decarboxylation reaction from an unsaturated FFA in the absence of H<sub>2</sub>, and was highly stable for oleic acid conversion selectively for green diesel production. However, a regenerative H<sub>2</sub> treatment was necessary to restore the catalytic activity and the desired product selectivity. Thus, Pd supported on carbon modified with silica may be regarded as a prospective decarboxylation catalyst for the removal of oxygen from vegetable oil/animal fat without the need of additional H<sub>2</sub>.

#### Acknowledgements

Financial support from the Department of Energy (Grant DEFG36-05G085005) and National Institute of Food and Agriculture (Grant MICW-2010-01534) for this research are gratefully acknowledged.

#### References

- [1] I. Simakova, O. Simakova, P. Maki-Arvela, A. Simakov, M. Estrada, D.Y. Murzin, *Appl. Catal. A: Gen.* 355 (2009) 100–108.
- [2] I. Simakova, O. Simakova, P. Maki-Arvela, D.Y. Murzin, *Catal. Today* 150 (2010) 28–31.
- [3] S. Lestari, P. Maki-Arvela, K. Eranen, J. Beltramini, G.Q.M. Lu, D.Y. Murzin, *Catal. Lett.* 134 (2010) 250–257.
- [4] E.W. Ping, R. Wallace, J. Pierson, T.F. Fuller, C.W. Jones, *Microporous Mesoporous Mater.* 132 (2010) 174–180.
- [5] E.W. Ping, J. Pierson, R. Wallace, J.T. Miller, T.F. Fuller, C.W. Jones, *Appl. Catal. A: Gen.* 396 (2011) 85–90.
- [6] M. Arend, T. Nonnen, W.F. Hoelderich, J. Fischer, J. Groos, *Appl. Catal. A: Gen.* 399 (2011) 198–204.
- [7] M. Snare, I. Kubickova, P. Maki-Arvela, K. Eranen, D.Y. Murzin, *Ind. Eng. Chem. Res.* 45 (2006) 5708–5715.
- [8] H. Bernas, K. Eranen, I. Simakova, A.R. Leino, K. Kordas, J. Myllyoja, P. Maki-Arvela, T. Salmi, D.Y. Murzin, *Fuel* 89 (2010) 2033–2039.
- [9] S. Lestari, P. Maki-Arvela, H. Bernas, O. Simakova, R. Sjöholm, J. Beltramini, G.Q.M. Lu, J. Myllyoja, I. Simakova, D.Y. Murzin, *Energy Fuels* 23 (2009) 3842–3845.
- [10] J.G. Immer, M.J. Kelly, H.H. Lamb, *Appl. Catal. A: Gen.* 375 (2010) 134–139.
- [11] J. Fu, X. Lu, P.E. Savage, *Energy Environ. Sci.* 3 (2010) 311–317.
- [12] R. Liu, Y. Shi, Y. Wan, Y. Meng, F. Zhang, D. Gu, Z. Chen, B. Tu, D. Zhao, *J. Am. Chem. Soc.* 128 (2006) 11652–11662.
- [13] Y. Wan, H. Wang, Q. Zhao, M. Klingstedt, O. Terasaki, D. Zhao, *J. Am. Chem. Soc.* 131 (2009) 4541–4550.
- [14] M.L. Anderson, R.M. Stroud, D.R. Rolison, *Nano Lett.* 2 (2002) 235.
- [15] V.Z. Radkevich, T.L. Senko, K. Wilson, L.M. Grishenko, A.N. Zaderko, V.Y. Diyuk, *Appl. Catal. A: Gen.* 335 (2008) 241–251.
- [16] B.K. Pradhan, N.K. Sandle, *Carbon* 37 (1999) 1323–1332.
- [17] M. Polovina, B. Babi, B. Kaluderovi, A. Dekanski, *Carbon* 35 (1997) 1047–1052.
- [18] H. Markus, A.J. Plomp, P. Maki-Arvela, J.H. Bitter, D.Y. Murzin, *Catal. Lett.* 113 (2007) 141–146.
- [19] H. Yang, Y. Yan, Y. Liu, F. Zhang, R. Zhang, Y. Meng, M. Li, S. Xie, B. Tu, D. Zhao, *J. Phys. Chem. B* 108 (2004) 17320–17328.
- [20] K.-W. Park, Y.-E. Sung, *J. Phys. Chem. B* 108 (2004) 939–944.
- [21] D.D. Kragten, J.M. Fedeyko, K.R. Sawant, J.D. Rimer, D.G. Vlachos, R.F. Lobo, *J. Phys. Chem. B* 107 (2003) 10006–10016.
- [22] M. Gurrath, T. Kuretzky, H.P. Boehm, L.B. Okhlopova, A.S. Lisitsyn, V.A. Likholobov, *Carbon* 38 (2000) 1241–1255.
- [23] N. Krishnakutty, M.A. Vannice, *J. Catal.* 155 (1995) 312–326.
- [24] K.S.W. Sing, D.H. Everett, R.A.W. Haul, L. Moscou, R.A. Pierotti, J. Rouquerol, T. Siemieniowska, *Pure Appl. Chem.* 57 (1985) 603–619.
- [25] L.C. Klein, in: J.L. Vossen, W. Kern (Eds.), *Thin Film Processes II*, Academic Press, Inc., San Diego, CA, 1991, pp. 501–520.
- [26] M.G.M. Van-Der-Vis, E.H.P. Cordfunke, R.J.M. Konings, *Journou De Physique IV Colloque C3, supplement au Journal de Physique* 11.3 (1993) 75.
- [27] A. Fukunaga, Y. Okayasu, Patent No. EP0495392A1, Ebara Corporation, Japan, 22 July 1992.
- [28] H.H. Tseng, M.Y. Wey, *Chemosphere* 62 (2006) 756–766.
- [29] M.L. Toebes, J.A.V. Dillen, K.P.D. Jong, *J. Mol. Catal. A: Chem.* 173 (2001) 75–98.
- [30] B.P. Tripathi, V.K. Shahi, *Prog. Polym. Sci.* 36 (2011) 945–979.
- [31] A.M. Seco, M.C. Goncalves, R.M. Almeida, *Mater. Sci. Eng. B76* (2000) 193–199.
- [32] R.M. Silverstein, F.X. Webster, *Spectrometric Identification of Organic Compounds*, sixth ed., John Wiley & Sons, Inc., New York, 1998, pp. 71–143.
- [33] P. Vinke, M.V.D. Eijk, M. Verbree, A.F. Voskamp, H.V. Bekkum, *Carbon* 32 (1994) 675–686.
- [34] M.S. Solum, R.J. Pugmire, M. Jagtoyen, F. Derbyshire, *Carbon* 33 (1995) 1247–1254.
- [35] M.B. Smith, J. March, *March's Advanced Organic Chemistry: Reactions, Mechanisms, and Structure*, 5th ed., Wiley-Interscience, 2001.
- [36] A.M. Puziy, O.I. Poddubnaya, A. Martinez-Alonso, F. Suarez-Garcia, J.M.D. Tascon, *Carbon* 40 (2002) 1493–1505.
- [37] J.P. d. Celis, M.S. Villaverde, A.L. Cukierman, N.E. Amadeo, *Latin Am. Appl. Res.* 39 (2009) 165–171.
- [38] H.-P. Boehm, *Angew. Chem. Int. Ed.* 5 (1966) 533–622.
- [39] M. Snare, I. Kubickova, P. Maki-Arvela, D. Chichova, K. Eranen, D.Y. Murzin, *Fuel* 87 (2008) 933–945.
- [40] H.H. Lamb, L. Sremaniak, J.L. Whitten, *Surf. Sci.* 607 (2013) 130–137.
- [41] S.B. Ziemecki, G.A. Jones, D.G. Swartzfager, R.L. Harlow, *J. Am. Chem. Soc.* 107 (1985) 4547.
- [42] R. Lamber, N. Jaeger, G. Schulz-Ekloff, *Surf. Sci.* 227 (1990) 15.
- [43] J.G. Immer, H.H. Lamb, *Energy Fuels* 24 (2010) 5291–5299.